JOURNAL OF THERMOPHYSICS AND HEAT TRANSFER
Vol. 28, No. 4, October–December 2014

Dynamic Heat Transfer Inside Multilayered Packages with Arbitrary Heat Generations

M. Fakoor-Pakdaman,* Mehran Ahmadi,† Farshid Bagheri,† and Majid Bahrami‡
Simon Fraser University, Surrey, British Columbia V3T 0A3, Canada

DOI: 10.2514/1.T4328

In most engineering applications, e.g., hybrid electric vehicles, the multilayered electronic packages generate arbitrary heat over a transient thermal duty cycle. In addition, the outer surface of such media endures time-dependent temperature as a result of variable coolant temperature during driving/duty cycles. As such, a new analytical model is developed to predict transient heat conduction inside multilayered composite media with arbitrary heat generation inside the layers. It is assumed that the temperature of the outer surface varies periodically over time. New compact closed-form relationships are developed for calculating 1) the temperature distribution inside multilayered media, 2) the average temperature of each layer, and 3) the interfacial heat flux. As an example, the methodology is applied to a two-concentric-cylinder composite. A detailed parametric study is conducted, and the critical values for the dimensionless parameters are evaluated; beyond these values, the temperature field inside the media is not affected considerably for any combination of other variables. It is shown that there is an optimum angular frequency that maximizes the amplitude of the interfacial heat flux. An independent numerical simulation is also performed using commercially available software ANSYS; the maximum relative difference between the obtained numerical data and the analytical model is less than 2%.

Nomenclature

A	=	matrix defined in Eq. (A5)
A_n	=	constant, Eqs. (A19) and (A20)
C_{jn}	=	integration coefficient, Eq. (A3)
D_{jn}	=	integration coefficient, Eq. (A3)
F	=	constant, Eq. (A8)
Fo	=	Fourier number, $\alpha_1 t/x_1^2$
G	=	arbitrary function of η, Eq. (A11)
G_n	=	constants defined in Eq. (A16)
H	=	constant, Eq. (A11)
h	=	contact conductance between layers, $\mathrm{W/m^2 \cdot K}$
i	=	complex variable, $\sqrt{-1}$
J_0	=	zero-order Bessel function of first kind
J_1	=	first-order Bessel function of first kind
K_j	=	dimensionless thermal conductivity ratio, k_{j+1}/k_j
k_j	=	thermal conductivity of the jth layer, $\mathrm{W/m \cdot k}$
M	=	number of layers
P	=	matrix defined in Eqs. (A5), (A6a), and (A6c)
p	=	integer number, where p is equal to 0, 1, and 2 for slabs, cylinders, and spheres, respectively
Q	=	matrix defined in Eqs. (A5), (A6b), and (A6d)
$q^*_{\eta_j}$	=	dimensionless interfacial heat flux at interface of jth layer, where η is equal to η_j, $(\partial\theta_j/\partial\eta)_{\eta_j=\frac{x_j}{x_1}}$
$\dot{q}$	=	volumetric heat generation inside jth layer, $\mathrm{W/m^3}$
R_{jn}	=	nth eigenfunction associated with λ_n for jth layer, Eq. (A1)
T_j	=	temperature of jth layer of composite media, K
t	=	time, s
w	=	weight function, Eqs. (A9)
x_M	=	space coordinate at outer-boundary surface
x_j	=	values of space coordinate at inner boundary surfaces, $j = 0, 1, 2, \ldots, M$, (m)
x_0	=	coordinate origin
Y_0	=	zero-order Bessel function of second kind
Y_1	=	first-order Bessel function of second kind
α_j	=	thermal diffusivity of jth layer, $\mathrm{m^2/s}$
Γ	=	function of Fourier number, Eq. (A13)
ΔT_R	=	amplitude of imposed temperature, K
$\Delta\varphi$	=	thermal lag
η	=	dimensionless coordinate, x/x_1
η_j	=	dimensionless coordinate at boundaries, x_j/x_1
θ	=	dimensionless temperature, $(T - T_0)/\Delta T_R$
θ_j	=	dimensionless temperature of jth layer, $(T_j - T_0)/\Delta T_R$
Λ_j	=	dimensionless contact conductance
λ	=	separation constant
λ_n	=	nth eigenvalue
μ_j	=	dimensionless thermal diffusivity ratio
ξ	=	dummy variable of the integral, Eq. (A21)
ϕ_{jn}	=	solution to Eq. (A1), corresponding to λ_n
ψ_{jn}	=	solution to Eq. (A1) corresponding to λ_n
Ω	=	angular frequency, rad/s
ω	=	dimensionless angular frequency

Subscripts

0	=	initial condition
j	=	jth layer defined in domain $x_{j-1} \le x \le x_j$, where j is equal to $1, 2, \ldots, M$
n	=	integer number, positive
R	=	reference value

Superscript

$'$	=	first derivative with respect to η

Received 21 November 2013; revision received 16 April 2014; accepted for publication 17 April 2014; published online 16 July 2014.

*Laboratory for Alternative Energy Conversion, School of Mechatronic Systems Engineering, #4300, 250-13450 102nd Avenue; mfakoorp@sfu.ca (Corresponding Author).

†Laboratory for Alternative Energy Conversion, School of Mechatronic Systems Engineering.

‡Laboratory for Alternative Energy Conversion, School of Mechatronic Systems Engineering; mbahrami@sfu.ca.

I. Introduction

INTEGRATION of component thermal management technologies for new propulsion systems is a key to developing innovative technology for the next-generation hybrid electric vehicles (HEVs), electric vehicles (EVs), and fuel cell vehicles (FCVs). Current hybrid systems use a separate cooling loop for the Power Electronics and Electric Machine (PEEM) [1,2]. However, using an integrated

cooling loop for a HEV addresses the cost, weight, size, and fuel consumption [2–4]. Typically, steady-state scenarios are considered for the thermal management of conventional vehicles [3,5]. However, within the context of integrated thermal management, the evaluation over transient thermal duty cycles is important because certain components may not experience peak thermal loads at the same time and over steady-state cases [2]. For critical semiconductor devices such as insulated gate bipolar transistors (IGBTs) in a HEV, McGlen et al. [6] predicted heat fluxes of 150–200 W/cm^2 and pulsed transient heat loads with heat fluxes up to 400 W/cm^2. One important aspect of the reliable thermal design of the dynamic multilayered systems of the PEEM is the ability to obtain an accurate transient temperature solution of the packages beforehand over a duty cycle in order to sustain the reliability of the packages, albeit for a more simplified configuration.

To successfully integrate the dynamic PEEM cooling systems concept into vehicle applications, the thermal limitations of the semiconductor devices must be addressed [7]. According to Samsung technologists, the next-generation semiconductor technology costs about $10 billion to create [7]. Alternatively, use of multilayered packages is recognized as an innovative technique for the thermal management of semiconductor devices, which also results in improved performance through the lowering of signal delays and increasing of processing speed. However, because of the dynamic unsteady characteristics of the power electronics inside HEVs/EVs/FCVs, accumulation of excessive heat within the multilayered packages is the main issue that needs to be addressed. This is attributed to the dynamic heat transfer characteristics as well as variable temperature of the interface of coolant and the composite over a duty cycle [7–9].

Transient heat conduction in a composite medium has been the subject of numerous studies, e.g., [8–28]. Different analytical approaches were adopted to analyze transient heat conduction in a multilayered composite including the Laplace transform method [12], quasi-orthogonal expansion technique [13–19], Green's function approach [20], and finite integral transform technique [21]. Tittle [14] presented the concept of quasi orthogonality, by which orthogonal eigensets are constructed from nonorthogonal ones in composite media. Recently, de Monte [23–28] published a series of papers on transient thermal characteristics of a composite slab under external convective cooling using a natural analytic approach [22]. He also described and compared the aforementioned analytical methods in [22]. Although encountered quite often in practice, time-dependent boundary conditions always posed challenge to the analysis of transient heat conduction in multilayered composites [23–25]. The pertinent literature has been limited to constant boundary conditions, i.e., isothermal, isoflux, or convective cooling. To the best of our knowledge, there are only few works on transient heat conduction in multilayered composites subjected to time-dependent boundary conditions and arbitrary heat generations; a summary of the literature is presented in Table 1. Our literature review indicates the following:

1) There is no model to predict the thermal behavior of a composite medium with heat generation under time-dependent boundary conditions.

2) The interfacial heat flux of a composite medium with heat generation has not been reported, when surface temperature varies periodically over time.

3) No model has been developed to determine optimum conditions that maximize the heat transfer rate of a composite multilayered system under arbitrary surface temperature.

4) No parametric study exists in the literature to investigate effects of the thermophysical and geometrical parameters on the heat transfer characteristics of composite media.

In this study, a new analytical model is developed for Cartesian, cylindrical, and spherical coordinates. The present model accurately predicts 1) the temperature distribution in the layers; 2) the average temperature of each layer; and 3) the interfacial heat flux, when an arbitrary temperature is imposed on the surface of a multilayered medium. Arbitrary heat generations inside each layer are taken into account. This paper provides an in-depth understanding of transient dynamic conduction inside a composite medium consisting of an arbitrary number of layers with different thermophysical properties. In particular, critical values for thermophysical and salient geometrical parameters are determined beyond which the temperature field is not affected considerably. Moreover, a set of optimum conditions is determined that establishes a maximum interfacial heat transfer rate.

To develop the present analytical model, a quasi-orthogonal expansion technique [14] is used. It is assumed that the boundary (surface) temperature varies harmonically. Following [16], a nonstandard method of separation of variables is employed, and all the layers are treated as one region with discontinuities at the interfaces. The associated discontinuous-weighting functions are found to make the resulting eigenfunctions orthogonal. As such, temperature distributions inside a multilayered region under cyclic temperature can be obtained. It is noteworthy that any type of arbitrary boundary condition can be decomposed into simple oscillatory functions using a Fourier series transformation [26]. Since the governing equations are linear, the results of this study can be extended to calculate the transient response of multilayered composite media under dynamically varying surface temperature, using a superposition technique.

II. Governing Equations

As mentioned before, for the sake of effective thermal management of multilayered packages inside Advanced Power Electronics and Electric Machines (APEEM) over a duty cycle, it is necessary to obtain the temperature distribution inside the packages, albeit for a more simplified configuration. Therefore, in this study, composite slabs, concentric cylinders, and spheres are taken into account as simplified geometries representing the thermal behavior of composite packages in APEEM. It should be noted that the coolant temperature varies dynamically over a duty cycle, which in turn results in a variable surface temperature of the composite packages.

Table 1 Summary of the existing models for unsteady multilayered conduction

Author(s)	Boundary condition	Notes
Mayer [13]	Convective cooling	✓ Reported temperature distribution inside a composite slab × No explanation for the orthogonality factors
Olek et al. [16]	Step surface temperature/heat flux	✓ Reported temperature distribution inside a composite cylinder Limited to a two-layer cylinder
Olek [18]	Convective cooling	✓ Reported temperature distribution for multiregion heat transfer in a generic coordinate system × Limited to homogeneous-type boundary conditions
De Monte [22]	Convective cooling	✓ Reported temperature distribution inside a composite medium in a generic coordinate × Limited to homogeneous-type boundary conditions
Lu et al. [23,24]	Time-dependent convective cooling	✓ Reported temperature distribution inside a composite cylinder/slab ✓ Developed a closed-form model for the transcendental equation of eigenvalues ✓ Did not consider heat generation inside the layers ✓ Complex Laplace-type integral equations should be solved to account for the time-dependent boundary condition

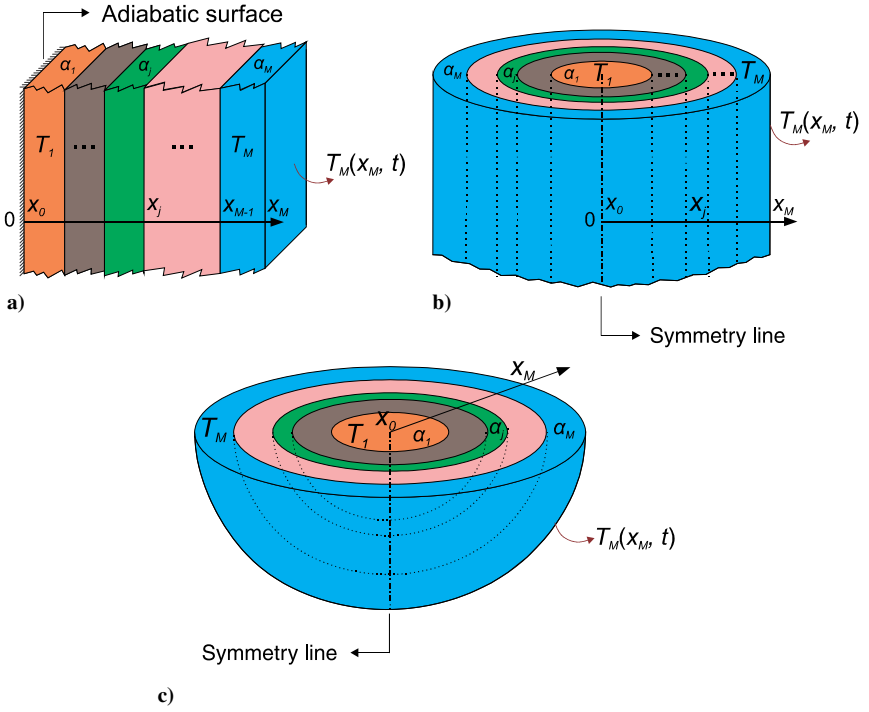

Fig. 1 Schematic of a multilayer composite in a) Cartesian, b) cylindrical, and c) spherical coordinate systems.

Therefore, the problem boils down to consideration of a multilayered package that undergoes a thermal transient as a result of arbitrary heat generations inside the layers and a dynamic outer-boundary temperature. Shown in Fig. 1 is a multilayered composite region involving M parallel layers, i.e., slabs, concentric cylinders, or spheres, respectively. We assume a perfect thermal contact between the layers, which results in the continuity of temperature and heat flux at the interfaces. The effect of thermal contact resistance between the layers for homogenized boundary conditions was studied by Ozisik [27] and can be applied to the present model as indicated in Appendix B of this study. In addition, without loss of generality, it is assumed that the surface x_0 represents the coordinate origin, $x_0 = 0$. In the case of composite slabs, $x = x_0$ is thermally insulated, while it is the symmetry line in case of concentric cylinders and the center in case of spheres. Moreover, the layer boundaries in the x direction are $x_1, x_2, \ldots, x_j$, where $j = 1, 2, \ldots, M$. Let k_j and α_j be the thermal conductivity and the thermal diffusivity of the jth layer, respectively. Initially, the body, which is confined to the domain $x_0 \le x \le x_M$, is at a uniform temperature T_0. Suddenly, at $t = 0$, the outer surface, $x = x_M$, is subjected to a periodic temperature varying in a cosine manner over time with an amplitude of ΔT_R:

$$T_M = T_0 + \Delta T_R \cos(\Omega t) \tag{1}$$

Other assumptions used in the proposed unsteady heat-conduction model are as follows:

1) There are constant thermophysical properties for all M layers.

2) The thickness of the multilayered solid is sufficiently thin in the x direction compared to the other directions, i.e., one-dimensional heat transfer.

As such, the mathematical formulation of the transient heat-conduction problem herein under discussion is

$$\nabla^2 T_j(x,t) = \frac{1}{\alpha_j}\frac{\partial T_j(x,t)}{\partial t} + \frac{\dot{q}_j(x)}{k_j} \qquad x_{j-1} \le x \le x_j, \quad t > 0, \quad j = 1, 2, \ldots, M \tag{2}$$

The boundary conditions are

$$\frac{\partial T_1(0,\,t)}{\partial x} = 0 \qquad \text{at } x = 0, \quad t > 0 \tag{3a}$$

$$T_j(x_j,t) = T_{j+1}(x_j,t) \quad j = 1,2,3,\ldots,(M-1) \text{ and } t > 0 \tag{3b}$$

$$k_j \frac{\partial T_j(x_j,\,t)}{\partial x} = k_{j+1}\frac{\partial T_{j+1}(x_j,\,t)}{\partial x} \qquad j = 1, 2, 3, \ldots, (M-1) \text{ and } t > 0 \tag{3c}$$

$$T_M(x_M, t) = T_0 + \Delta T_R \cos(\Omega t) \quad \text{at } x = x_M, \quad t > 0 \tag{3d}$$

The initial condition is

$$T_j(x,0) = T_0 \qquad x_{j-1} \le x \le x_j, \quad j = 1, 2, \ldots, M, \quad \text{and} \quad t = 0 \tag{3e}$$

where

$$\nabla^2 \equiv \frac{1}{x^p}\frac{\partial}{\partial x}\left(x^p \frac{\partial}{\partial x}\right) \tag{4}$$

is the one-dimensional Laplace differential operator and ΔT_R [K] and Ω [rad/s] are the amplitude and the angular frequency of the imposed temperature at the outer surface, $x = x_M$, respectively. It should be noted that p takes the values of 0, 1, and 2, for Cartesian, cylindrical, and spherical coordinate systems, respectively.

We define the following dimensionless variables:

$$Fo = \frac{\alpha_1 t}{x_1^2}, \qquad \eta = \frac{x}{x_1}, \qquad \mu_j = \frac{\alpha_j}{\alpha_1},$$

$$g_j(\eta) = \mu_j \frac{\dot{q}(x)_j x_1^2}{k_j \Delta T_R}, \quad K_j = \frac{k_{j+1}}{k_j}, \quad \theta = \frac{T - T_0}{\Delta T_R}, \quad \omega = \Omega \frac{x_1^2}{\alpha_1}$$

Therefore, the dimensionless form of Eq. (2) becomes

$$\frac{\partial\theta_j}{\partial Fo}=\mu_j\frac{1}{\eta^p}\frac{\partial}{\partial\eta}\left(\eta^p\frac{\partial\theta_j}{\partial\eta}\right)+g_j(\eta)\qquad 0\le\eta\le\frac{x_M}{x_1},\quad Fo>0$$
$$j=1,2,\ldots,M \tag{5}$$

subjected to the following dimensionless boundary conditions:

$$\frac{\partial\theta_1}{\partial\eta}=0\quad\text{at }\eta=0,\qquad Fo>0 \tag{6a}$$

$$\theta_j(\eta=x_j/x_1,Fo)=\theta_{j+1}(\eta=x_j/x_1,Fo)$$
$$j=1,2,3,\ldots,(M-1),\quad\text{and}\quad Fo>0 \tag{6b}$$

$$\frac{\partial\theta_j(\eta=x_j/x_1,Fo)}{\partial\eta}=K_j\frac{\partial\theta_{j+1}(\eta=x_j/x_1,Fo)}{\partial\eta}$$
$$j=1,2,3,\ldots,(M-1),\ \text{and}\ Fo>0 \tag{6c}$$

$$\theta_M=\cos(\omega Fo)\quad\text{at }\eta=\frac{x_M}{x_1},\qquad Fo>0 \tag{6d}$$

The dimensionless initial condition inside the medium is

$$\theta_j(\eta,0)=0\qquad\frac{x_{j-1}}{x_1}\le\eta\le\frac{x_j}{x_1},\qquad j=1,2,3,\ldots,M$$
$$\text{and}\quad Fo=0 \tag{6e}$$

It should be noted that, conceptually, the Fourier number Fo is the ratio of diffusive/conductive transport rate by the quantity storage rate and arises from nondimensionalization of the heat equation, see [27] for more detail.

III. Model Development

A new model is developed to predict the thermal response of a multilayered composite in Cartesian, cylindrical, and spherical coordinates under periodic time-dependent surface temperatures. The methodology is presented for 1) a composite medium with an arbitrary number of layers, see Appendix A, and then 2) two concentric cylinders as examples; a similar approach can be taken for other geometries and layers. In should be noted that the one-dimensional unsteady heat-conduction model developed here cannot be applied to nonaxisymmetric composite cylinders and spheres.

In Appendix A, a general solution is presented for a one-dimensional transient heat-conduction problem inside a multilayered composite medium of M layers with different thermophysical and geometrical properties, subjected to a periodic boundary temperature at the outer surface. The solution is presented in Cartesian, cylindrical, and spherical coordinate systems. In this section, as a solution example, the aforementioned methodology is applied to investigate the transient thermal response of two concentric cylinders. With reference to Table 2, for the case of a two-region cylinder, $p=1$ and $M=2$, the eigenfunctions are as given as

Table 2 The linearly independent solutions $\phi_{jn}(\eta)$ and $\psi_{jn}(\eta)$ of Eq. (A3) for different geometries

P (geometry)	$\phi_{in}(\eta)$	$\psi_{in}(\eta)$
0 (Cartesian)	$\cos\left(\frac{\lambda_n\eta}{\sqrt{\mu_j}}\right)$	$\sin\left(\frac{\lambda_n\eta}{\sqrt{\mu_j}}\right)$
1 (cylindrical)	$J_0\left(\frac{\lambda_n\eta}{\sqrt{\mu_j}}\right)$	$Y_0\left(\frac{\lambda_n\eta}{\sqrt{\mu_j}}\right)$
2 (spherical)	$\frac{1}{\eta}\sin\left(\frac{\lambda_n\eta}{\sqrt{\mu_j}}\right)$	$\frac{1}{\eta}\cos\left(\frac{\lambda_n\eta}{\sqrt{\mu_j}}\right)$

$$R_n(\eta)=\begin{cases}R_{1n}=J_0(\lambda_n\eta)\\ R_{2n}=C_{2n}J_0(\lambda_n\eta/\sqrt{\mu_2})+D_{2n}Y_0(\lambda_n\eta/\sqrt{\mu_2})\end{cases} \tag{7}$$

Applying the boundary conditions and taking Eq. (A4) into consideration, the matrices A and v can be determined as

$$A=\begin{bmatrix}J_0(\lambda_n) & -J_0\left(\frac{\lambda_n}{\sqrt{\mu_2}}\right) & -Y_0\left(\frac{\lambda_n}{\sqrt{\mu_2}}\right)\\ -J_1(\lambda_n) & \frac{K_1}{\sqrt{\mu_2}}\times J_1\left(\frac{\lambda_n}{\sqrt{\mu_2}}\right) & \frac{K_1}{\sqrt{\mu_2}}\times Y_1\left(\frac{\lambda_n}{\sqrt{\mu_2}}\right)\\ 0 & J_0\left(\frac{\lambda_n\eta_2}{\sqrt{\mu_2}}\right) & Y_0\left(\frac{\lambda_n\eta_2}{\sqrt{\mu_2}}\right)\end{bmatrix}_{3\times3} \tag{8}$$

$$v=[\,1\quad C_{2n}\quad D_{2n}\,]^T \tag{9}$$

where η_2 denotes the thickness ratio, i.e., $\eta_2=x_2/x_1$. Based on Eq. (A7), the following transcendental equation is obtained to evaluate the eigenvalues:

$$-\frac{Y_0(\lambda_n\eta_2/\sqrt{\mu_2})}{J_0(\lambda_n\eta_2/\sqrt{\mu_2})}=\frac{[J_0(\lambda_n)\times Y_1(\lambda_n/\sqrt{\mu_2})]-(\sqrt{\mu_2}/K_1)\times[Y_0(\lambda_n/\sqrt{\mu_2})\times J_1(\lambda_n)]}{[(\sqrt{\mu_2}/K_1)\times J_0(\lambda_n/\sqrt{\mu_2})\times J_1(\lambda_n)]-[J_0(\lambda_n)\times J_1(\lambda_n/\sqrt{\mu_2})]} \tag{10}$$

The constants C_{2n} and D_{2n} are evaluated by applying Eq. (A4):

$$C_{2n}=\frac{[J_0(\lambda_n)\times Y_1(\lambda_n/\sqrt{\mu_2})]-(\sqrt{\mu_2}/K_1)\times[Y_0(\lambda_n/\sqrt{\mu_2})\times J_1(\lambda_n)]}{[J_0(\lambda_n/\sqrt{\mu_2})\times Y_1(\lambda_n/\sqrt{\mu_2})]-[Y_0(\lambda_n/\sqrt{\mu_2})\times J_1(\lambda_n/\sqrt{\mu_2})]} \tag{11a}$$

$$D_{2n}=\frac{(\sqrt{\mu_2}/K_1)\times[J_0(\lambda_n/\sqrt{\mu_2})\times J_1(\lambda_n)]-[J_0(\lambda_n)\times J_1(\lambda_n/\sqrt{\mu_2})]}{[J_0(\lambda_n/\sqrt{\mu_2})\times Y_1(\lambda_n/\sqrt{\mu_2})]-[Y_0(\lambda_n/\sqrt{\mu_2})\times J_1(\lambda_n/\sqrt{\mu_2})]} \tag{11b}$$

Using Eqs. (A9) and (A10), the following relationships are obtained to find the discontinuous-weighting functions:

$$w(x)=\frac{\eta}{\mu_j}F_j,\qquad F_1=1,\qquad F_2=K_1\quad j=1,2 \tag{12}$$

Thus, with respect to Eq. (A19), the temperature distribution inside the entire medium is obtained as

$$\theta_j(\eta,Fo)=\cos(\omega Fo)+\sum_{n=1}^{\infty}R_{jn}(\eta)\left\{\begin{matrix}A_n e^{-(\lambda_n^2 Fo)}-\\ E_n\left[\frac{\omega\times\cos(\omega Fo)-\lambda_n^2\times\sin(\omega Fo)}{\lambda_n^4+\omega^2}\right]+\frac{G_n}{\lambda_n^2}\end{matrix}\right\}$$
$$j=1,2 \tag{13}$$

where R_{1n} and R_{2n} are evaluated by Eq. (7) and the coefficients A_n are obtained by Eq. (A20). Moreover, regarding Eq. (A15), the coefficients E_n can be obtained as follows:

$$E_n=\omega\times\frac{\int_0^1\eta R_{1n}(\eta)\,d\eta+\frac{K_1}{\mu_2}\int_1^{\eta_2}\eta R_{2n}(\eta)\,d\eta}{\int_0^1\eta R_{1n}^2(\eta)\,d\eta+\frac{K_1}{\mu_2}\int_1^{\eta_2}\eta R_{2n}^2(\eta)\,d\eta} \tag{14}$$

As indicated by Eq. (A21), the average temperature of the inner cylinder can be determined by the following relationship:

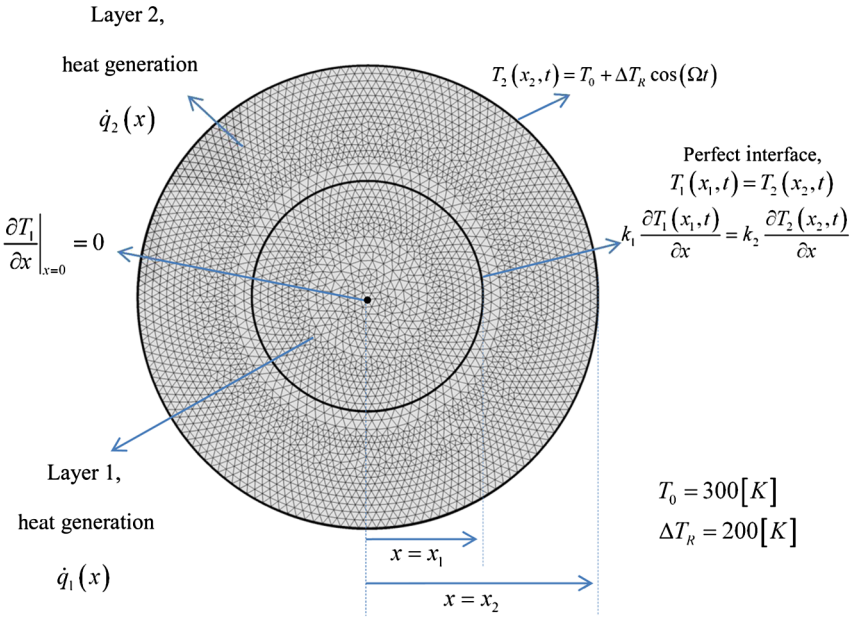

Fig. 2 Numerical domain and the grid sizes for the base case.

$$\bar{\theta}_1(\omega, Fo) = \cos(\omega Fo) + \sum_{n=1}^{\infty} \frac{J_1(\lambda_n)}{\lambda_n} \left\{ \begin{array}{l} A_n e^{-(\lambda_n^2 Fo)} - \\ E_n \left[\frac{\omega \times \cos(\omega Fo) - \lambda_n^2 \times \sin(\omega Fo)}{\lambda_n^4 + \omega^2} \right] + \frac{G_n}{\lambda_n^2} \end{array} \right\} \quad (15)$$

The interfacial heat flux for this case can be obtained by the following equation, see Eq. (A22):

$$q^*_{\eta_1} = \left.\frac{\partial \theta_1}{\partial \eta}\right|_{\eta_1 = 1} = \sum_{n=1}^{\infty} [-\lambda_n \times J_1(\lambda_n)] \left\{ \begin{array}{l} A_n e^{-(\lambda_n^2 Fo)} - \\ E_n \left[\frac{\omega \times \cos(\omega Fo) - \lambda_n^2 \times \sin(\omega Fo)}{\lambda_n^4 + \omega^2} \right] + \frac{G_n}{\lambda_n^2} \end{array} \right\} \quad (16)$$

It can be shown that at the limit where $\omega \to 0$, i.e., the isothermal outer-boundary temperature, Eq. (13) reduces to

$$\theta_j(\eta, Fo) = 1 + \sum_{n=1}^{\infty} R_{jn}(\eta) \left[I_n e^{-(\lambda_n^2 Fo)} + \frac{G_n}{\lambda_n^2} \right] \quad j = 1, 2 \quad (17)$$

where

$$I_n = -\frac{\int_0^1 \eta R_{1n}(\eta)\, d\eta + \frac{K_1}{\mu_2} \int_1^{\eta_2} \eta R_{2n}(\eta)\, d\eta}{\int_0^1 \eta R_{1n}^2(\eta)\, d\eta + \frac{K_1}{\mu_2} \int_1^{\eta_2} \eta R_{2n}^2(\eta)\, d\eta} - \frac{G_n}{\lambda_n^2} \quad (18)$$

Equation (17) is the solution to the temperature distribution inside two concentric cylinders with heat generation under the step (isothermal) surface temperature as represented by Olek et al. [16].

In addition, when $\omega \to 0$, without heat generations $g_j(\eta) = 0$, and the same thermophysical properties for both layers, Eq. (13) reduces to

$$\theta(\eta, Fo) = 1 - 2 \sum_{n=1}^{\infty} \frac{J_0(\lambda_n \eta)}{\lambda_n \eta_2 J_1(\lambda_n \eta_2)} \times \exp(-\lambda_n^2 Fo) \quad (19)$$

where λ_n are the positive roots of $J_0(\lambda_n \eta_2)$; see Eq. (10). This is the solution for the temperature distribution inside a solid cylinder of infinite length, subjected to a step (isothermal) surface temperature; e.g., see Carslaw and Jaeger [12].

IV. Numerical Study

To verify the proposed analytical solution, an independent numerical simulation of the unsteady one-dimensional heat conduction inside two concentric cylinders is conducted using the commercial software ANSYS. A user-defined code (UDF) is written to apply the periodic surface temperature, Eq. (1). Furthermore, the assumptions stated in Sec. II are used in the numerical analysis. Grid independency of the results is also verified by using three different grid sizes, namely, 1878, 6362, and 12,000 cells. Since there was a little difference between the simulation results from the fine- and medium-sized grids (only 1% at the most), the medium grid size was chosen for modeling to reduce the computational time. Besides, in the numerical analysis, the thermal contact resistance between the layers is neglected. In other words, it is assumed that there is a perfect thermal contact between the layers, as indicated by Eq. (3c). The numerical domain, boundary conditions, and the corresponding mesh are shown in Fig. 2. The geometrical and thermal properties used in the baseline case for the numerical simulation are listed in Table 3. The maximum relative difference between the analytical results and the numerical data is less than 2%, which is discussed in detail in Sec. V.

V. Parametric Study

In this section, a comprehensive parametric study is conducted to investigate the effects of different parameters on the thermal response of a multilayered composite medium. The analytical results obtained in Sec. III for two concentric cylinders are represented here in graphical form and compared with the numerical data obtained in Sec. IV. As such, the effect of various dimensionless parameters on the thermal characteristics of the system is studied. The dimensionless variables affecting the thermal behavior of the system are 1) heat generation, 2) the thermal conductivity ratio, 3) the thermal diffusivity ratio, 4) the thickness ratio, and 5) the angular frequency of the imposed surface temperature.

Table 3 Values of the thermal and geometrical properties for the baseline case in the numerical simulation

Layer, j	Density ρ, kg/m^3	Thermal conductivity k, W/m/K	Thermal capacity c_p, J/kg/K	Thickness x, m
1	100	400	1000	0.1
2	100	100	1000	0.1

$T_0 = 300$ K, $\Delta T_R = 200$ K

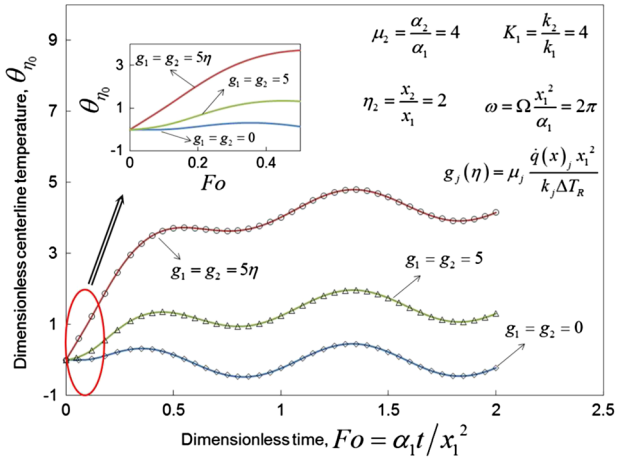

Fig. 3 Variations of the dimensionless centerline temperature, Eq. (13), against the Fo number for different types of heat generation inside the layers.

A code is developed using commercial software Maple 15 to solve the transcendental relationship, Eq. (10). Our study shows that using the first 50 terms in the series solution, Eq. (10), is accurate enough to obtain the temperature distribution inside the media up to four decimal digits. Note that the estimated number of series terms can notably be reduced for large time scales since, for large values of n, $\lambda_n \to \infty$, and the exponential term in Eq. (13) drops remarkably.

A. Effect of Heat Generation

Figure 3 shows the variations of the centerline temperature against the Fo number for different types of heat generation inside the layers. Three different cases are considered separately to show the effect of heat generation and verify the presented analytical solution. Definitions of cases 1 and 2 are indicated in Table 4, while for case 3, the heat generation inside the layers is equal to zero. Lines in Fig. 3 represent the analytical solutions, and the symbols are used to indicate the numerical simulation results. According to Table 3, the following values are assumed arbitrarily for other dimensionless variables: $K_1 = k_2/k_1 = 4$, $\mu_2 = \alpha_2/\alpha_1 = 4$, $\omega = 2\pi$, and $\eta_2 = x_2/x_1 = 2$. The same trend is observed for any other combination of these parameters, and thus they can be adopted as general results. The values of thermophysical and geometrical parameters for the numerical analysis are previously presented in Table 3. In addition, the dimensional and dimensionless values of heat generation considered in this section for analytical and numerical studies are shown in Table 4. As seen from Fig. 3, there is a good agreement between the numerical data and the analytical results, a maximum relative difference of less than 1.5%. The following conclusions can be drawn from Fig. 3:

1) At very initial times, as the heat generation inside the layers increases, the thermal lag of the system decreases. Therefore, as $Fo \to 0$ and $g_1 = g_2 = 0$, it takes some time for the centerline to respond to the temperature excitation at the outer boundary. However, the trend is a complete reverse for the case in which $Fo \to 0$ and $g_j \neq 0$.

2) Regardless of the heat generation inside the layers, the temperature inside the media fluctuates with the agitation angular frequency of the outer boundary.

Table 4 Dimensional and corresponding dimensionless heat generations considered in the numerical and analytical models, respectively

	Case 1		Case 2	
Heat generation	Dimensionless value g_j	Numerical value $\dot{q}_j$, W/m^3	Dimensionless value g_j	Numerical value, W/m^3
First layer, $j = 1$	5η	$400 \times 10^6 x$	5	$40 \times 10^6 x$
Layer 2, $j = 2$	5η	$400 \times 10^6 x$	5	$40 \times 10^6 x$

$\Omega = 0.8\pi$ rad/s

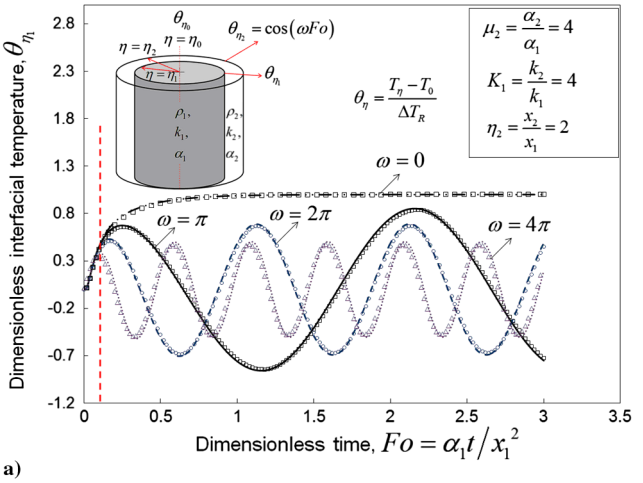

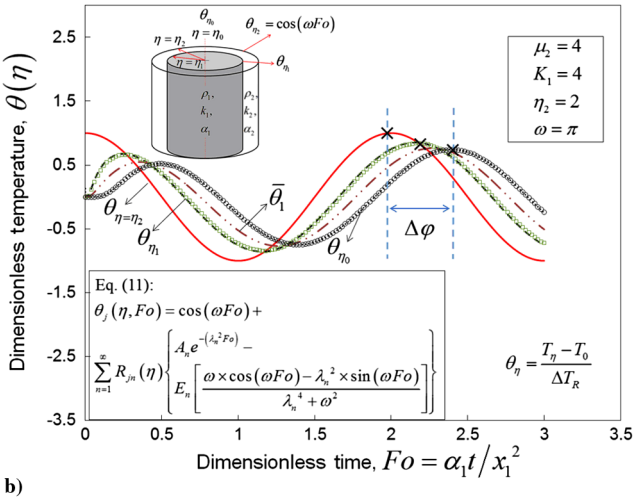

Fig. 4 Effects of angular frequency on a) interfacial temperature, and b) temperature field, vs the Fo number.

B. Effect of Angular Frequency

Figure 4 shows the temperature field inside concentric cylinders vs the Fo number for different values of the angular frequency, Eqs. (13) and (15). Lines in Fig. 4 represent the analytical solutions, and the symbols are used to indicate the numerical simulation results. The following values are assumed arbitrarily for other dimensionless variables: $K_1 = k_2/k_1 = 4$, $\mu_2 = \alpha_2/\alpha_1 = 4$, and $\eta_2 = x_2/x_1 = 2$. The values of thermophysical and geometrical parameters for the numerical analysis are presented in Table 3. The dimensionless angular frequency for the analytical study is considered as $\omega = 0, \pi, 2\pi$, and 4π, which are corresponding to the dimensional angular frequency of Ω rad/s $= 0, 0.4\pi, 0.8\pi$, and 1.6π, respectively, for the numerical analysis. From Fig. 4, one can see that there is an excellent agreement between the analytical results, Eqs. (13) and (15), and the obtained numerical data. The maximum relative difference is less than 2%. Also, the angular frequency of the imposed boundary temperature has a significant effect on the thermal response of the multilayered composite media. Further, the following conclusions can be drawn:

1) As $\omega \to 0$, the imposed boundary temperature becomes constant with time. Therefore, the present model yields the solution of the step boundary temperature, i.e., Eq. (17).

2) As the angular frequency of the imposed temperature increases, temperature fields do not follow the details of the imposed surface temperature. As a result, the amplitudes of the temperature profiles inside the media decrease.

3) The frequency of the temperature field inside the system is the same as the frequency of the imposed surface temperature.

4) At early times, $Fo < 0.05$, the temperature inside the media is not a function of the angular frequency. As such, all the curves for

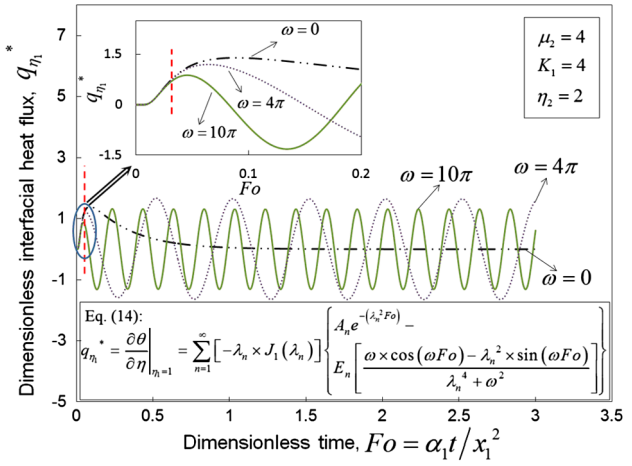

Fig. 5 Variations of the dimensionless interfacial heat flux versus the Fo number (dimensionless time).

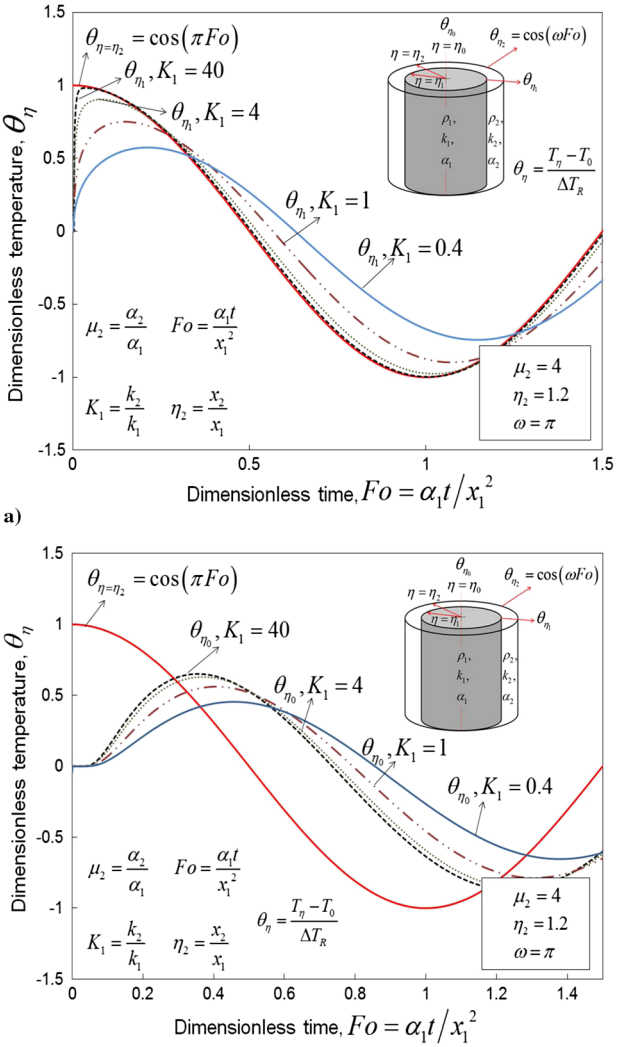

Fig. 6 Effects of thermal conductivity ratio on a) interfacial and b) centerline temperatures vs the Fo number.

different values of the angular frequency follow the same line, i.e., the step surface temperature, $\omega \to 0$. This region is demarcated by the dashed line in Fig. 4a.

5) The shift between the peaks of the temperature profiles is marked at different radial positions. This shows a thermal lag due to the thermal inertia of the system, which increases toward the centerline of the concentric cylinder $\Delta\varphi$.

Figure 5 shows the dimensionless interfacial heat flux vs the Fo number for different values of the angular frequency, Eq. (16). One can conclude the following from Fig. 5:

1) At the limit where $\omega \to 0$, i.e., the step surface temperature, the dimensionless interfacial heat flux reaches a maximum and then decreases remarkably to reach a plateau at zero as $Fo \to \infty$. It should be noted that when the step surface temperature is imposed on the outer boundary the entire media reach the imposed temperature as $Fo \to \infty$. Therefore, the interfacial heat flux becomes zero for large Fo numbers.

2) When $\omega \neq 0$, the interfacial heat flux acts periodically over time with the frequency of the imposed surface temperature.

3) As the angular frequency increases to a certain value, the amplitude of the interfacial heat flux increases notably. This is called the optimum angular frequency, which maximizes the interfacial heat flux. This is discussed in more detail in Sec. V.F.

4) As previously mentioned, at early times, $Fo < 0.05$, all the curves for different angular frequencies branch off from the same line, i.e., the step surface temperature where $\omega \to 0$. This region is demarcated by the dashed line in Fig. 5.

C. Effect of Thermal Conductivity Ratio, $K_1 = k_1/k_2$

Figures 6a and 6b show the variations of the interfacial and centerline temperature vs the Fo number for different values of the thermal conductivity ratio. The solid red line shows the imposed surface temperature at the boundary. The following values are assumed arbitrarily for other dimensionless variables: $\mu_2 = \alpha_2/\alpha_1 = 4$, $\eta_2 = x_2/x_1 = 1.2$, and $\omega = \pi$. From Fig. 6, the following can be concluded:

1) As the thermal conductivity ratio increases, the thermal lag of the system decreases significantly.

2) The more the thermal conductivity ratio, the higher the amplitude of the temperature inside the medium.

3) As the thermal conductivity ratio increases, the interfacial temperature approaches the imposed surface temperature, i.e., the red line in Figs. 6a and 6b.

4) There is a considerable thermal lag between the interfacial and centerline temperatures due to the thermal inertia of the inner cylinder.

5) The change in the temperature distribution inside the medium is not significant for $K_1 > 4$. This can be called the critical thermal conductivity ratio beyond which for any combination of the other parameters the calculated values of the temperature are not affected by more than 1.4%, $K_{cr} = 4$.

Variations of the dimensionless interfacial heat flux, Eq. (16), vs the Fo number for different values of the thermal conductivity ratio are plotted in Fig. 7. From Fig. 7, the following conclusions can be drawn:

1) The amplitude of the interfacial heat flux increases with the thermal conductivity ratio.

2) Increasing the thermal conductivity ratio beyond its critical value, $K_{cr} = 4$, does not affect the interfacial heat flux significantly. The maximum relative difference between the interfacial heat fluxes for $K = 4$ and $K = 100$ is less than 1.4%.

3) As the thermal conductivity ratio decreases, the amount of heat conducted from the outer layer to the inner one drops significantly. Therefore, the outer surface acts as a thermal insulator, and the interfacial heat flux drops down considerably.

4) Therefore, for $K_1 \geq 1$, the interfacial heat flux approaches the imposed heat flux at the outer boundary due to the high thermal conductivity of the outer cylinder. However, the amplitude of the interfacial heat flux for $K_1 = 0.4$ is dramatically less than that of $K_1 \geq 1$.

D. Effect of Thermal Diffusivity Ratio, $\mu_2 = \alpha_2/\alpha_1$

Figures 8a–8c show the interfacial temperature; centerline temperature, Eq. (13); and interfacial heat flux, Eq. (16), respectively, vs the Fo number for different values of the thermal diffusivity ratio. The following values are assumed arbitrarily for other dimensionless variables: $K_1 = k_2/k_1 = 4$, $\eta_2 = x_2/x_1 = 2$, and $\omega = \pi$. From Fig. 8, one can conclude the following:

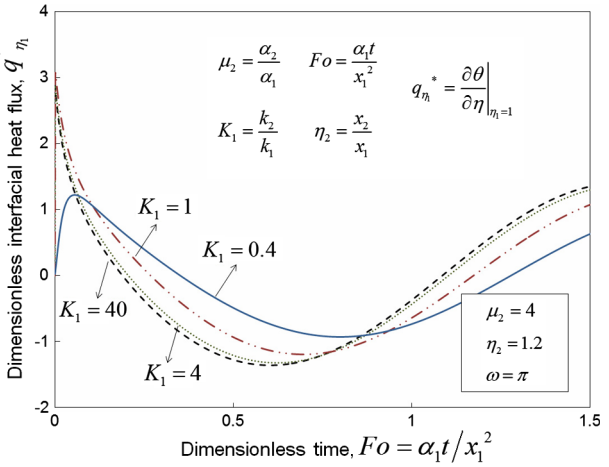

Fig. 7 Interfacial heat flux vs the *Fo* number for different values of the thermal conductivity ratio, Eq. (16).

1) As the thermal diffusivity ratio increases, the thermal lag of the system decreases significantly.

2) Increasing the thermal diffusivity ratio augments the amplitude of the temperature inside the media.

3) The critical value for the thermal diffusivity ratio is $\mu_{cr}=40$. Beyond this value, for any combination of the other parameters, the temperature field inside the medium is not affected considerably. For instance, for $\mu=40$ and $\mu=100$, the maximum relative difference for the interface temperature is less than 0.9%.

4) As the thermal diffusivity ratio drops, the amount of heat diffused from the outer layer to the inner one decreases. Therefore, the outer surface acts as a thermal insulator, and the amplitude of the interfacial heat flux goes down considerably.

E. Effect of Thickness Ratio, $\eta_2 = x_2/x_1$

Figures 9a–9c show the interfacial temperature; centerline temperature, Eq. (13); and interfacial heat flux, Eq. (16), respectively, vs the Fo number for different values of the thickness ratio. The following values are assumed arbitrarily for other dimensionless variables: $K_1=k_2/k_1=4$, $\mu_2=\alpha_2/\alpha_1=4$, and $\omega=\pi$. One can conclude the following from Fig. 9:

1) As the thickness ratio increases, the thermal lag of the system increases notably.

2) The thermal inertia of the outer surface increases with the thickness ratio. Therefore, as the thickness ratio increases, the amplitude of the interfacial temperature/heat flux decreases remarkably.

3) The interfacial temperature approaches the imposed surface temperature as the thickness ratio decreases.

4) Regardless of the thickness ratio, the temperature inside the multilayered region oscillates with the same frequency of the imposed surface temperature.

F. Angular Frequency to Maximize Interfacial Heat Flux

As pointed out earlier in Sec. V.D, for given values of the dimensionless parameters K_1, μ_2, and η_2, there is an optimum value for the angular frequency at which the amplitude of the interfacial heat flux is maximum. Figure 10 shows the variations of the maximum amplitude of interfacial heat flux, $q^*_{\max,\eta=\eta_1}$, vs the angular frequency for different values of the thickness ratio, η_2. Here, the values of the thermal conductivity and diffusivity ratios are chosen arbitrarily equal to 4. It should be noted that $q^*_{\max,\eta=\eta_1}$ shows the maximum amplitude of interfacial heat flux over the entire time (see Fig. 4). The following conclusions can be drawn from Fig. 10:

1) As the angular frequency increases, the maximum amplitude of interfacial heat flux, $q^*_{\max,\eta=\eta_1}$, at first decreases slightly. However, after a certain point, it starts increasing to form a hump at the optimum angular frequency range. Beyond the optimum point, the interfacial heat flux decreases until it asymptotically approaches zero.

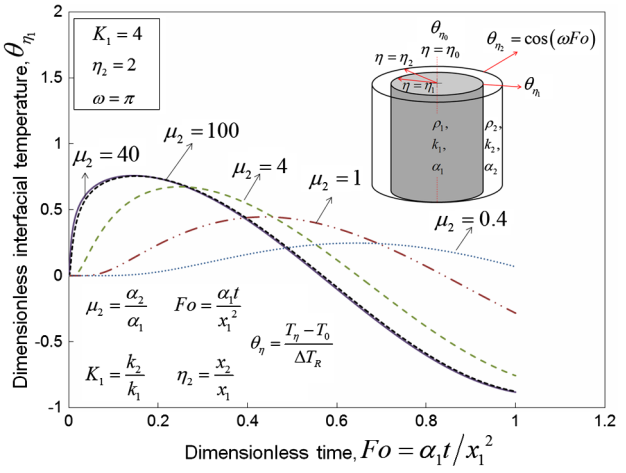

a)

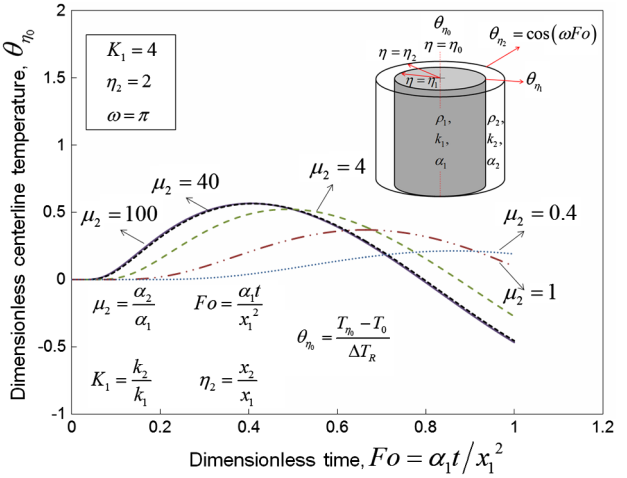

b)

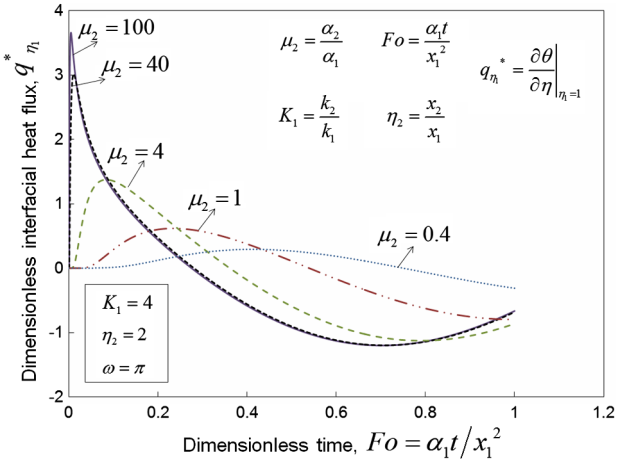

c)

Fig. 8 Effects of thermal diffusivity ratio on a) interfacial and b) centerline temperatures, and c) interfacial heat flux.

2) For given values of thermal conductivity, thermal diffusivity, and the thickness ratio, there is an optimum angular frequency that maximizes the amplitude of the interfacial heat flux, i.e., $q^*_{\eta=\eta_1}$. These points are marked on Fig. 10.

3) To find the optimum angular frequency, for a given set of properties, one should use Eq. (A22). Accordingly, variations of the interfacial heat flux vs angular frequency are obtained for different geometrical and thermophysical properties, which in turn reveal the optimum angular frequency that maximizes the amplitude of the interfacial heat flux.

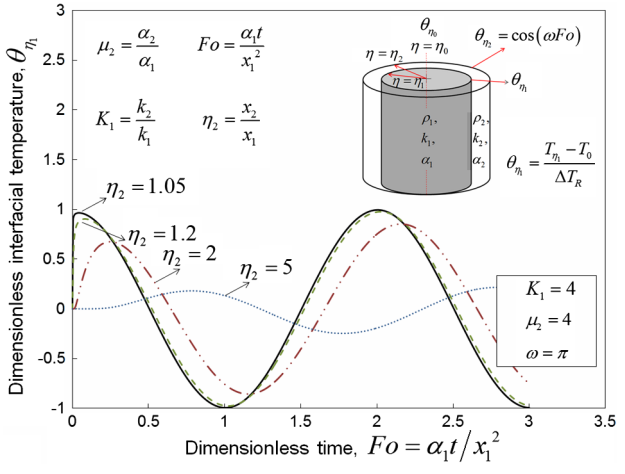

a)

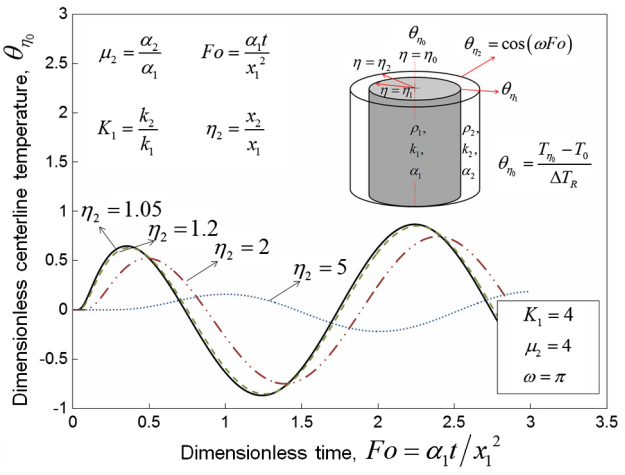

b)

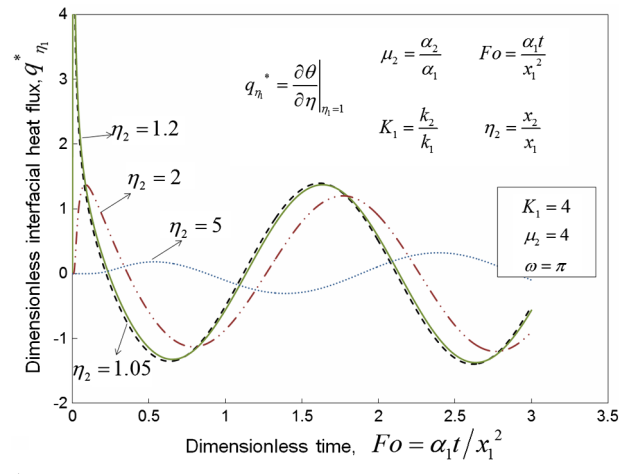

c)

Fig. 9 Effects of thickness ratio on a) interfacial temperature, b) centerline temperature, and c) interfacial heat flux.

4) For some specific cases, e.g., $K_1 = 4$ and $\mu_2 = 4$, the following relationship can be obtained between the maximum interfacial heat flux and the angular frequency.

5) As an example, for $K_1 = 4$ and $\mu_2 = 4$, based on curve fitting the maximum interfacial heat flux can be correlated to the angular frequency by the following relationship:

$$q^*_{\eta_1,\max}(\omega) = 0.07\omega + 0.95 \tag{20}$$

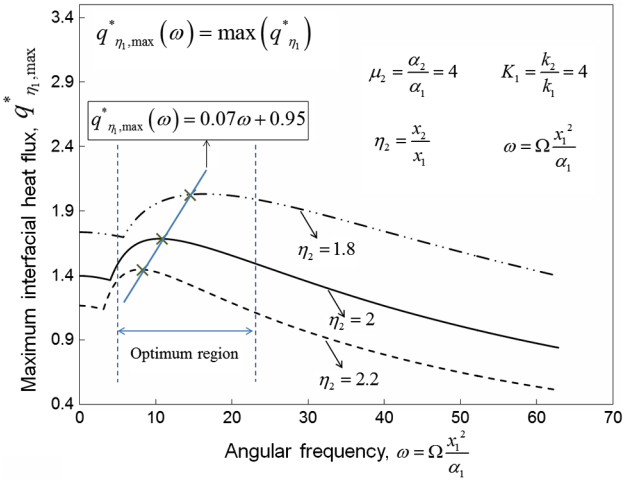

Fig. 10 Variations of the maximum interfacial heat flux vs the angular frequency.

VI. Conclusions

A new analytical model is presented for the solution of one-dimensional heat diffusion inside a multilayered composite medium with an arbitrary number of layers under periodic outer-surface temperature. The solution is presented in a generic coordinate to account for heat conduction inside composite slabs, concentric cylinders, or spheres. A nonstandard method of the separation of variables is applied, which treats the entire multilayered region as one domain with certain discontinuities at the interfaces between layers. Closed-form relationships are proposed to predict 1) temperature distribution inside the media, 2) the average temperature of each layer, and 3) the interfacial heat flux. The present analytical results are verified successfully with the obtained independent numerical data. The maximum relative difference between the analytical results and the numerical data is less than 2%. As an example, the methodology is applied to investigate the thermal characteristics of two concentric cylinders under the periodic outer-surface temperature. The highlights of the present study can be listed as the following:

1) The main dimensionless parameters characterizing the thermal behavior of a composite medium are 1) the thermal diffusivity ratio, 2) the thermal conductivity ratio, 3) the thickness ratio, and 4) the dimensionless angular frequency.

2) Because of the thermal inertia of the system, there is a shift, or thermal lag, between the temperature profiles at different radial positions; this increases toward the centerline as the thermal inertia increases.

3) At two limiting cases, the thermal response of the system yields that of the step surface temperature: 1) $Fo \to 0$ (early time) and 2) no thermal fluctuations, $\omega \to 0$.

4) As thermal conductivity or diffusivity ratios increase, the thermal lag of the system decreases. As a result, the interfacial temperature becomes closer to the imposed surface temperature.

5) There are critical values for the dimensionless thermal conductivity and diffusivity ratios beyond which the temperature field inside the medium is not affected considerably for any combination of the other parameters.

6) For given values of thermal conductivity, thermal diffusivity, and the thickness ratio, there is an optimum value for the angular frequency at which the interfacial heat flux reaches its maximum value.

Appendix A: *M*-Layer Composite

The system of eigenvalue problems associated with Eq. (5) is given as

$$\mu_j \frac{1}{\eta^p}\frac{\mathrm{d}}{\mathrm{d}\eta}\left(\eta^p \frac{\mathrm{d}R_{jn}}{\mathrm{d}\eta}\right) = -\lambda_n^2 R_{jn} \qquad j = 1, 2, 3, \ldots, M \tag{A1}$$

with the homogenous boundary conditions

$$\frac{\partial R_1}{\partial \eta} = 0 \quad \text{at } \eta = 0 \tag{A2a}$$

$$R_j(\eta = x_j/x_1) = R_{j+1}(\eta = x_j/x_1) \quad j = 1,2,3,\ldots,(M-1) \tag{A2b}$$

$$\frac{\partial R_j(\eta = x_j/x_1)}{\partial \eta} = K_j \frac{\partial R_{j+1}(\eta = x_j/x_1)}{\partial \eta} \qquad j = 1, 2, 3, \ldots, (M-1) \tag{A2c}$$

$$R_M = 0 \quad \text{at } \eta = \frac{x_M}{x_1} \tag{A2d}$$

where R_{jn} is the eigenfunction in the jth layer associated with the nth eigenvalue λ_n. The general solution of the previously mentioned eigenvalue problem is in the form of

$$R_{jn}(\eta) = \begin{cases} R_{1n}(\eta) = \phi_{1n}(\eta) & 0 \le \eta \le 1 \\ R_{jn}(\eta) = C_{jn}\phi_{jn}(\eta) + D_{jn}\psi_{jn}(\eta) & \dfrac{x_{j-1}}{x_1} \le \eta \le \dfrac{x_j}{x_1} \\ & j = 2, 3, \ldots, M \end{cases} \tag{A3}$$

where the functions $\phi_{jn}(\eta)$ and $\psi_{jn}(\eta)$ are two linearly independent solutions of Eq. (A1). Table 2 lists the function $\phi_{jn}(\eta)$ and $\psi_{jn}(\eta)$ for slabs, cylinders, and spheres.

It should be noted that J_0 and Y_0 are zeroth-order Bessel functions of the first and second kinds, respectively. Furthermore, the $\psi_{1n}(\eta)$ function is excluded from the solution, Eq. (A3), because of the boundary condition at the origin; see Eq. (6a). The remaining boundary conditions, Eqs. (6b–6f), yield

$$Av = 0 \tag{A4}$$

where $v = [1, C_{2n}, D_{2n}, C_{3n}, D_{3n}, \ldots, C_{Mn}, D_{Mn}]^T$ and the matrix A is defined by

$$A = \begin{bmatrix} P_1 & 0 & 0 & 0 & 0 & 0 \\ Q_1 & 0 & 0 & 0 & 0 & 0 \\ 0 & P_2 & 0 & 0 & 0 & 0 \\ 0 & Q_2 & 0 & 0 & 0 & 0 \\ \vdots & \vdots & \vdots & \ldots & \vdots & \vdots \\ \vdots & \vdots & \vdots & \ldots & \vdots & \vdots \\ 0 & 0 & 0 & 0 & 0 & P_{M-1} \\ 0 & 0 & 0 & 0 & 0 & Q_{M-1} \\ 0 & 0 & 0 & 0 & 0 & P_M \end{bmatrix}_{(2M-1)\times(2M-1)} \tag{A5}$$

where

$$P_1 = [\,\phi_{1n} \quad -\phi_{2n} \quad -\psi_{2n}\,]_{\text{at } \eta=1} \tag{A6a}$$

$$Q_1 = [\,\phi'_{1n} \quad -K_1\phi'_{2n} \quad -K_1\psi'_{2n}\,]_{\text{at } \eta=1} \tag{A6b}$$

$$P_j = [\,\phi_{jn} \quad \psi_{jn} \quad -\phi_{(j+1)n} \quad -\psi_{(j+1)n}\,]_{\text{at } \eta=\frac{x_j}{x_1}}, \qquad j = 2, 3, \ldots, (M-1) \tag{A6c}$$

$$Q_j = [\,\phi'_{jn} \quad \psi'_{jn} \quad -K_j\phi'_{(j+1)n} \quad -K_j\psi'_{(j+1)n}\,]_{\text{at } \eta=\frac{x_j}{x_1}}, \qquad j = 2, 3, \ldots, (M-1) \tag{A6d}$$

$$P_M = [\,\phi_{Mn} \quad \psi_{Mn}\,]_{\text{at } \eta=\frac{x_M}{x_1}} \tag{A6e}$$

Equation (A4) yields $2M-1$ homogenous simultaneous equations for v_j, $j = 1, 2, 3, \ldots, M$. A nontrivial solution exists if the determinant of the coefficients is zero:

$$\det A = 0 \tag{A7}$$

Equation (A7) can be solved for the eigenvalues λ_n. For each value of λ_n that satisfies Eq. (A7), only $2M-2$ of the $2M-1$ equations in Eq. (A4) are linearly independent so that $2M-2$ unknowns can be obtained from these equations in terms of the remaining ones. Following [16] and [28], as indicated by Eq. (A3), without loss of generality, the value of the constants multiplied by ϕ_{1n} and C_{1n} are taken as unity so that the coefficients $C_{2n}, D_{2n}, \ldots, C_{Mn}, D_{Mn}$ can be determined. Taking C_{1n} as unity will not affect the solution since all the components of the solution are normalized [16]. The eigenfunctions $R_{jn}(\eta)$ do not form an orthogonal set due to the discontinuity of the first derivative of $R_{jn}(\eta)$ at the interfaces, i.e., $\eta = x_j/x_1$, $j = 1, 2, \ldots, (M-1)$, Eq. (A3). Therefore, the Strum–Liouville theorem of orthogonality cannot be applied. However, the functions can be made orthogonal with respect to a discontinuous-weighting function, which can be found by the method introduced by Yeh [15]. The method is not presented here; one can refer to [15] and [18] for more details. To apply the method, we rewrite Eq. (A1) in the following form:

$$\frac{\mathrm{d}}{\mathrm{d}\eta}\left(F_j\eta^p \frac{\mathrm{d}R_{jn}}{\mathrm{d}\eta}\right) + \lambda_n^2\eta^p \frac{F_j}{\mu_j}R_{jn} = 0 \qquad \frac{x_{j-1}}{x_1} \le \eta \le \frac{x_j}{x_1}, \qquad j = 1, 2, 3, \ldots, M \tag{A8}$$

Note that F_j is a constant within the interval $x_{j-1}/x_1 \le \eta \le x_j/x_1$, yet unknown. Based on [15] and [18], the constants F_j should be determined such that the functions R_{jn} become orthogonal with respect to the discontinuous-weighting function $w(\eta)$. As such, the orthogonality factors are given as

$$w(\eta) = \frac{\eta^p}{\mu_j}F_j \quad \frac{x_{j-1}}{x_1} \le \eta \le \frac{x_j}{x_1}, \qquad j = 1, 2, \ldots, M \tag{A9}$$

Following Yeh [15], the following relationship is developed to evaluate the constants F_j, to form the weighting functions:

$$F_1 = 1, \qquad F_j = \prod K_{j-1} \qquad j = 2, 3, \ldots, M \tag{A10}$$

Now that the constants F_j are determined, the weighting function $w(\eta)$ is known. Therefore, any function $G(\eta)$ can be expanded inside the entire multilayered medium as follows:

$$G(\eta) = \sum_{n=1}^{\infty} H_n R_n(\eta) \qquad 0 \le \eta \le \frac{x_M}{x_1} \tag{A11}$$

The expansion is carried out over the range of $0 \le \eta \le x_M/x_1$, spanning all M layers. The unknown coefficients H_n in Eq. (A11) are determined by a generalized Fourier analysis over the entire range of M layers and are given in the following form:

$$H_n = \frac{\sum_{j=1}^{M} \int_{\text{layer}j} G(\eta) w(\eta) R_{jn}(\eta)\, \mathrm{d}\eta}{\sum_{j=1}^{M} \int_{\text{layer}j} w(\eta)[R_{jn}(\eta)]^2\, \mathrm{d}\eta} \tag{A12}$$

Therefore, after using a separation-of-variables method, the temperature distribution inside the entire media is considered in the form

$$\theta_j(\eta, Fo) = e^{i\omega Fo} + \sum_{n=1}^{\infty} R_{jn}(\eta)\Gamma(Fo)e^{i\omega Fo} \quad j = 1,2,\ldots,M \tag{A13}$$

where $i = \sqrt{-1}$. The choice of using a complex exponential function comes from the nature of the problem since we know that regardless of the heat generation the temperature inside the media fluctuates with the angular frequency of the boundary. Clearly, the final solution is the real part of the sought-after solution. Substituting Eq. (A13) into Eq. (5) and expanding the angular frequency over the entire medium, after some algebraic manipulation, one obtains

$$\sum_{n=1}^{\infty} R_{jn}[\Gamma'(Fo) + (i\omega + \lambda_n^2)\Gamma(Fo) + iE_n - G_n \times e^{-i\omega Fo}] = 0 \tag{A14}$$

Where, based on Eq. (A12), the coefficients E_n and G_n can be determined by the following:

$$E_n = \omega \times \frac{\sum_{j=1}^{M} \int_{\text{layer}j} w(\eta) R_{jn}(\eta)\, \mathrm{d}\eta}{\sum_{j=1}^{M} \int_{\text{layer}j} w(\eta)[R_{jn}(\eta)]^2\, \mathrm{d}\eta} \tag{A15}$$

$$G_n = \frac{\sum_{j=1}^{M} \int_{\text{layer}j} g_j(\eta) w(\eta) R_{jn}(\eta)\, \mathrm{d}\eta}{\sum_{j=1}^{M} \int_{\text{layer}j} w(\eta)[R_{jn}(\eta)]^2\, \mathrm{d}\eta} \tag{A16}$$

Since in general R_{jn} is not zero, we must have

$$\Gamma'(Fo) + (i\omega + \lambda_n^2)\Gamma(Fo) + iE_n - G_n \times e^{-i\omega Fo} = 0 \tag{A17}$$

The solution of Eq. (A17) is given by

$$\Gamma(Fo) = A_n e^{-(\lambda_n^2 + i\omega)Fo} - \frac{E_n(\omega + i\lambda_n^2)}{\lambda_n^4 + \omega^2} + \frac{G_n}{\lambda_n^2} \times e^{-i\omega Fo} \tag{A18}$$

Substituting Eq. (A18) into Eq. (A13) and considering the real part of the solution,

$$\theta_j(\eta, Fo) = \cos(\omega Fo) + \sum_{n=1}^{\infty} R_{jn}(\eta) \left\{ \begin{array}{l} A_n e^{-(\lambda_n^2 Fo)} - \\ E_n \left[\frac{\omega \times \cos(\omega Fo) - \lambda_n^2 \times \sin(\omega Fo)}{\lambda_n^4 + \omega^2} \right] + \frac{G_n}{\lambda_n^2} \end{array} \right\} \quad j = 1, 2, \ldots, M \tag{A19}$$

The coefficients A_n can be obtained by using the initial condition, Eq. (6e), together with the orthogonality properties of the eigenfunctions:

$$A_n = E_n \left[\frac{\omega}{\omega^2 + \lambda_n^4} - \frac{1}{\omega} \right] - \frac{G_n}{\lambda_n^2} \tag{A20}$$

As remarked earlier, the constants E_n can be determined by Eq. (A15). The average temperature inside each layer is defined as

$$\bar{\theta}_j = \frac{1}{\eta_j^p - \eta_{j-1}^p} \int_{\xi=\eta_{j-1}}^{\eta_j} \xi^p \theta_j\, \mathrm{d}\xi \qquad j = 1, 2, \ldots, M \tag{A21}$$

where ξ is a dummy variable. Moreover, the dimensionless heat flux at interfaces can be obtained as follows:

$$q_j^* = \left.\frac{\partial \theta_j}{\partial \eta}\right|_{\eta_j = \frac{x_j}{x_1}} = \sum_{n=1}^{\infty} R'_{jn}(\eta_j) \left\{ \begin{array}{l} A_n e^{-(\lambda_n^2 Fo)} - \\ E_n \left[\frac{\omega \times \cos(\omega Fo) - \lambda_n^2 \times \sin(\omega Fo)}{\lambda_n^4 + \omega^2} \right] + \frac{G_n}{\lambda_n^2} \end{array} \right\} \quad j = 1, 2, \ldots, M-1 \tag{A22}$$

Appendix B: Consideration of Thermal Contact Resistance Between Layers

Although throughout this study the effect of thermal contact resistance (TCR) is neglected, in this section following [27], guidelines are provided to show how the thermal contact resistance between the layers can be treated. Therefore, only the equations that need to be modified to include the effects of TCR are shown here, and other equations remain the same. As such, Eq. (3b) should be altered to indicate the discontinuity of temperature at the interfaces as a result of TCR as

$$-k_j \frac{\partial T_j}{\partial x} = h_j \times [T_j(x_j, t) - T_{j+1}(x_j, t)] \quad j = 1,2,3,\ldots,(M-1) \text{ and } t > 0 \tag{B1}$$

where h_j $\mathrm{W/m^2\,K}$ is the contact conductance between the jth and $j+1$th layers. In addition, the dimensionless form of Eq. (B1) should be used instead of Eq. (6b),

$$\frac{\partial \theta_j}{\partial \eta} = \Lambda_j[\theta_{j+1}(\eta = x_j/x_1, Fo) - \theta_j(\eta = x_j/x_1, Fo)] \quad j = 1, 2, 3, \ldots, (M-1), \quad \text{and} \quad Fo > 0 \tag{B2}$$

where $\Lambda_j = \frac{h_j x_1}{k_j}$ is the dimensionless contact conductance between the jth and $j+1$th layers. Accordingly, the continuity of eigenfunction at the interface, Eq. (A2b), is modified as follows:

$$\frac{\partial R_j}{\partial \eta} = \Lambda_j[R_{j+1}(\eta = x_j/x_1) - R_j(\eta = x_j/x_1)] \quad j = 1, 2, 3, \ldots, (M-1) \tag{B3}$$

The matrices P_1 and P_j are obtained by the following relationships:

$$P_1 = \left[\frac{\phi'_{1n}}{\Lambda_1} - \phi_{2n} - \psi_{2n} \right]_{\text{at } \eta=1} \tag{B4}$$

$$P_j = \left[\frac{\phi'_{jn}}{\Lambda_j} \frac{\psi'_{jn}}{\Lambda_j} - \phi_{(j+1)n} - \psi_{(j+1)n} \right]_{\text{at } \eta = \frac{x_j}{x_1}}, \quad j = 2, 3, \ldots, (M-1) \tag{B5}$$

It should be noted that matrices Q_1, Q_j, and P_M do not change since they are not related to the thermal contact resistance between the layers. In this regard, the effect of contact resistance is reflected in the coefficients C_{jn} and D_{jn}, while, following the same procedure outlined in Appendix A, the temperature distribution inside the composite can be obtained. As such, if we apply the modified model to account for the TCR in a two-layer concentric cylinder, the temperature distribution inside the layer is obtained by Eq. (13), in which the modified transcendental equation is as

$$-\frac{Y_0(\lambda_n\eta_2/\sqrt{\mu_2})}{J_0(\lambda_n\eta_2/\sqrt{\mu_2})} = \frac{[J_0(\lambda_n)\times Y_1(\lambda_n/\sqrt{\mu_2})] - (\sqrt{\mu_2}/K_1)\times[Y_0(\lambda_n/\sqrt{\mu_2})\times J_1(\lambda_n)] - (\frac{\lambda_n}{\Lambda_1})\times[J_1(\lambda_n)Y_1(\lambda_n/\sqrt{\mu_2})]}{(\sqrt{\mu_2}/K_1)\times[J_0(\lambda_n/\sqrt{\mu_2})\times J_1(\lambda_n)] - [J_0(\lambda_n)\times J_1(\lambda_n/\sqrt{\mu_2})] + (\frac{\lambda_n}{\Lambda_1})[J_1(\lambda_n)J_1(\lambda_n/\sqrt{\mu_2})]} \tag{B6}$$

The values of C_{2n} and D_{2n} are obtained by the following relationships:

$$C_{2n} = \frac{[J_0(\lambda_n)\times Y_1(\lambda_n/\sqrt{\mu_2})] - (\sqrt{\mu_2}/K_1)\times[Y_0(\lambda_n/\sqrt{\mu_2})\times J_1(\lambda_n)] - (\frac{\lambda_n}{\Lambda_1})\times[J_1(\lambda_n)Y_1(\lambda_n/\sqrt{\mu_2})]}{[J_0(\lambda_n/\sqrt{\mu_2})\times Y_1(\lambda_n/\sqrt{\mu_2})] - [Y_0(\lambda_n/\sqrt{\mu_2})\times J_1(\lambda_n/\sqrt{\mu_2})]} \tag{B7}$$

$$D_{2n} = \frac{(\sqrt{\mu_2}/K_1)\times[J_0(\lambda_n/\sqrt{\mu_2})\times J_1(\lambda_n)] - [J_0(\lambda_n)\times J_1(\lambda_n/\sqrt{\mu_2})] + (\frac{\lambda_n}{\Lambda_1})[J_1(\lambda_n)J_1(\lambda_n/\sqrt{\mu_2})]}{[J_0(\lambda_n/\sqrt{\mu_2})\times Y_1(\lambda_n/\sqrt{\mu_2})] - [Y_0(\lambda_n/\sqrt{\mu_2})\times J_1(\lambda_n/\sqrt{\mu_2})]} \tag{B8}$$

The coefficients C_{2n} and D_{2n} show up in the eigenfunctions, Eq. (7), while other parameters can be obtained by the same procedure outlined earlier. It is evident that when $\Lambda_1 \to \infty$ the TCR becomes negligible, and the modified model in Appendix B becomes similar to that of Appendix A.

Acknowledgments

This work was supported by Automotive Partnership Canada, grant number APCPJ 401826-10. The authors would like to thank the support of the industry partner, Future Vehicle Technologies, Inc. (British Columbia, Canada).

References

[1] O'Keefe, M., and Bennion, K., "A Comparison of Hybrid Electric Vehicle Power Electronics Cooling Options," *Vehicle Power and Propulsion Conference*, Inst. of Electrical and Electronics Engineers, Arlington, TX, Sept. 2007, pp. 116–123. doi:10.1109/VPPC.2007.4544110.

[2] Bennion, K., and Thornton, M., "Integrated Vehicle Thermal Management for Advanced Vehicle Propulsion Technologies," *Society of Automotive Engineers (SAE) 2010 World Congress*, NREL Paper CP-540-47416, Denver, CO, Feb. 2010.

[3] Bennion, K., and Kelly, K., "Rapid Modeling of Power Electronics Thermal Management Technologies," *5th Institute of Electrical and Electronics Engineers Vehicle Power and Propulsion Conference*, NREL Paper CP-540-46172, Denver, CO, Aug. 2009.

[4] Bennion, K., and Thornton, M., "Integrated Vehicle Thermal Management for Advanced Vehicle Propulsion Technologies," *SAE 2010 World Congress*, NREL Paper CP-540-47416, Denver, CO, Feb. 2010.

[5] Panão, M. R. O., Correia, A. M., and Moreira, A. L. N., "High-Power Electronics Thermal Management with Intermittent Multijet Sprays," *Applied Thermal Engineering*, Vol. 37, May 2012, pp. 293–301.

[6] McGlen, R. J., Jachuck, R., and Lin, S., "Integrated Thermal Management Techniques for High Power Electronic Devices," *Applied Thermal Engineering*, Vol. 24, Nos. 8, 9, June 2004, pp. 1143–1156.

[7] Ghalambor, S., Agonafer, D., and Haji-Sheikh, A., "Analytical Thermal Solution to a Nonuniformly Powered Stack Package With Contact Resistance," *Journal of Heat Transfer*, Vol. 135, No. 11, Sept. 2013, p. 1–9.

[8] Wang, C. Y., "Heat Conduction Across a Sandwitched Plate with Stringers," *Journal of Thermophysics and Heat Transfer*, Vol. 8, No. 3, 1994, pp. 622–624.

[9] Han, L. S., "Periodic Heat Conduction Through Composite Panels," *Journal of Thermophysics and Heat Transfer*, Vol. 1, No. 2, 1986, pp. 184–186.

[10] Cheng, W.-L., Li, H., Liu, N., Huang, J.-R., Han, H.-Y., and Pang, S., "Thermal Performance Analysis of Space Debris Protection Enhanced Multilayer Perforated Insulation," *Journal of Thermophysics and Heat Transfer*, Vol. 24, No. 4, Oct. 2010, pp. 833–838.

[11] Padovan, J., "Generalized Strum-Liouville Procedure for Composite Domain Anisotropic Transient Conduction Problems," *Journal of Thermophysics and Heat Transfer*, Vol. 12, No. 1, 1974, pp. 1158–1160.

[12] Carslaw, H. S., and Jaeger, J. C., *Conduction of Heat in Solids*, Oxford Univ. Press, Oxford, England, U.K., 1959, p. 199.

[13] Mayer, E., "Heat Flow in Composite Slabs," *ARS Journal*, Vol. 22, No. 3, 1952, pp. 150–158.

[14] Tittle, C. W., "Boundary Value Problems in Composite Media: Quasi-Orthogonal Functions," *Applied Physics*, Vol. 36, 1965, pp. 1487–1488.

[15] Yeh, H. C., "Solving Boundary Value Problems in Composite Media by Separation of Variables and Transient Temperature of a Reactor Vessel," *Nuclear Engineering and Design*, Vol. 36, No. 2, 1976, pp. 139–157.

[16] Olek, S., Elias, E., Wacholder, E., and Kaizerman, S., "Unsteady Conjugated Heat Transfer in Laminar Pipe Flow," *International Journal of Heat and Mass Transfer*, Vol. 34, No. 6, 1991, pp. 1443–1450.

[17] Olek, S., "Heat Transfer in Duct Flow of Non-Newtonian Fluid with Axial Conduction," *International Communications in Heat and Mass Transfer*, Vol. 25, No. 7, 1998, pp. 929–938.

[18] Olek, S., "Multiregion Conjugate Heat Transfer," *Hybrid Methods in Engineering*, Vol. 1, No. 2, 1999, pp. 119–137.

[19] Olek, S., and Elias, E., "2-D Conjugate Heat Transfer in Fluids with an Arbitrary Fully-Developed Velocity Distribution," Institution of Chemical Engineers Symposium Series, Vol. 135, No. 4, 1994.

[20] Feng, Z. G., and Michaelides, E. E., "The Use of Modified Green's Functions in Unsteady Heat Transfer," *International Journal of Heat and Mass Transfer*, Vol. 40, No. 12, 1997, pp. 2997–3002.

[21] Yener, Y., and Ozisik, M. N., "On the Solution of Unsteady Heat Conduction in Multi-Region Finite Media with Time-Dependent Heat Transfer Coefficient," *Proceedings of 5th International Heat Transfer Conference, (A75-14226 03-34)*, Society of Heat Transfer of Japan, Tokyo, 1974, pp. 188–192.

[22] De Monte, F., "Transient Heat Conduction in One-Dimensional Composite Slab. A 'natural' Analytic Approach," *International Journal of Heat and Mass Transfer*, Vol. 43, No. 19, Oct. 2000, pp. 3607–3619.

[23] Lu, X., Tervola, P., and Viljanen, M., "Transient Analytical Solution to Heat Conduction in Composite Circular Cylinder," *International Journal of Heat and Mass Transfer*, Vol. 49, Nos. 1, 2, Jan. 2006, pp. 341–348.

[24] Lu, X., and Tervola, P., "Transient Heat Conduction in the Composite Slab-Analytical Method," *Journal of Physics A: General Physics*, Vol. 38, No. 1, 2005, pp. 81–96.

[25] Jain, P. K., and Singh, S., "Analytical Solution to Transient Asymmetric Heat Conduction in a Multilayer Annulus," *Journal of Heat Transfer*, Vol. 131, No. 1, 2009, Paper 011304.

[26] Kreyszig, E., Kreyzig, H., and Norminton, E. J., *Advanced Engineering Mathematics*, John Wiley and Sons, New York, 2012, pp. 473–492.

[27] Ozisik, M. N., *Boundary Value Problems of Heat Conduction*, International Textbook, London, 1968, pp. 262–294.

[28] De Monte, F., "An Analytic Approach to the Unsteady Heat Conduction Processes in One-Dimensional Composite Media," *International Journal of Heat and Mass Transfer*, Vol. 45, No. 6, Mar. 2002, pp. 1333–1343.